Validation of Theoretical Performance Results using Wave Tank Testing of Heaving Point Absorber Wave Energy Conversion Device working against a Subsea Reaction Plate

Mirko Previsic, mirko@re-vision.net
Kourosh Shoele, kourosh@re-vision.net
Jeff Epler, jeff@re-vision.net

Re Vision Consulting, Sacramento, CA, USA

ABSTRACT

The aim of this study was to validate different theoretical performance models using subscale wave tank tests. The device modeled is a heaving point absorber working against a submerged reaction plate. This type of device has been pursued by a number of commercial and is therefore relevant as a benchmark for future efforts on similar devices.

A set of model tests were carried out at 1:33 scale in the hydraulic laboratory at Scripps Institute of Oceanography. Wave periods between 5 and 20 seconds were selected to test the response of the model to sinusoidal waves. This corresponds roughly to the range of wave periods encountered at most deployment sites of interest globally.

A novel viscous damper was developed as part of the project to represent the power take-off, which provides a means to model a power take-off with virtually no friction and a very predictable behavior. This is an important consideration when trying to correlate wave tank tests and theoretical models.

Two theoretical models (1DoF and 3DoF) were developed in the commercial code AQWA and their results were compared to the model tests. Finally, a wave to wire model was developed to compute annual power production at a target deployment location in Northern California allowing for benchmarking of the machine.

The results show that good agreement between theoretical models and model testing can be attained if viscous drag terms are represented accurately.

INTRODUCTION

The aim of most wave energy conversion device developers is to build a machine that can produce electricity at the lowest cost of electricity possible. The calculation of the cost of electricity of a power plant is done by dividing the annualized cost of the plant by the annual power production. Hence, the accurate prediction of the performance for wave energy conversion is of critical importance to understand the commercial viability of the system.

The performance assessment process for a wave energy conversion device can be roughly divided into the following steps: (1) wave to mechanical energy conversion, (2) mechanical to electrical energy conversion, and (3) quantification of losses due to transmission losses, and plant availability. This study primarily focused on the first step within this assessment sequence.

The device studied is a heaving point absorber, which generates power from the relative motion between a surface float and a subsea reaction plate. This type of device was chosen, because it closely corresponds to devices under development by industry and hence is a good candidate for a benchmarking study. A review of devices and approaches can be found in [3].

The aim of this study was to; (1) establish a first-order data-set from subscale testing in a wave tank, and (2) validate a numerical performance models using these tests. The model was developed using AQWA, a commercial code developed by ANSYS. The code obtains hydrodynamic parameters using a boundary element method (BEM) in the frequency domain and then uses these within the AQWA commercial time-domain solver.

WAVE TANK SETUP

The wave tank at Scripps Institute of Oceanography was used to perform the testing. The wave tank is 30m long, 2.4m wide and 2.5m deep. The tank features glass-walls allowing users to observe device motion. An analog signal was used to control the hydraulic piston-type wave maker and generate the test waves. A carriage travels the length of the tank and was locked at 14 m from the wave maker for the testing and as an observation platform.
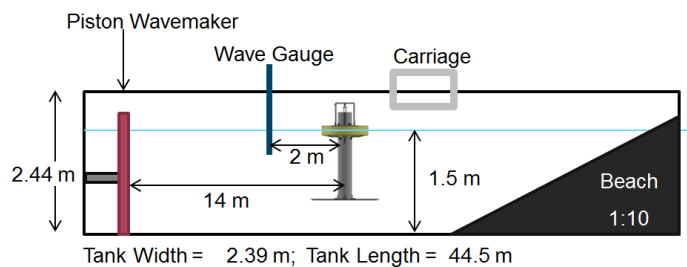

Figure 1 – Wave Tank Dimensions (not to scale)

DEVICE DIMENSIONS

Device dimensions, masses, moments of inertia, and mooring line spring-stiffness were developed from a concept-level design effort previously completed by efforts under the Department of Energy Reference Model Program. Froude scaling was used to scale the full-scale device to model scale.

The 1:33 scale model was built using syntactic foam for the float and aluminum for the central pipe, and the reaction plate. The scale was

chosen to accommodate the wave tank wave-making capabilities and match them to the full-scale range of variables to be tested. The power take off (PTO) was located inside the central pipe of the float to keep the center of gravity (Cg) as low as possible to maximize upright stability. The mass breakdown of all the components is given in Table 1. To match the inertia of the full scale device, 12 individual weights were machined to the mass specification and embedded in the float. The center of mass of the entire model is shown below with the reference origin at the center plane and center line of the damping plate.
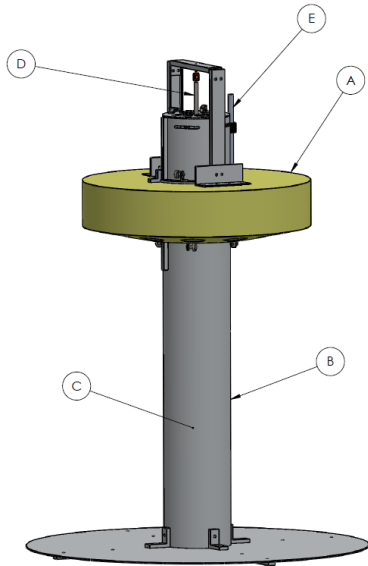

Figure 2 - Model Component Mass Key

Table 1 – Model Component Mass Breakdown

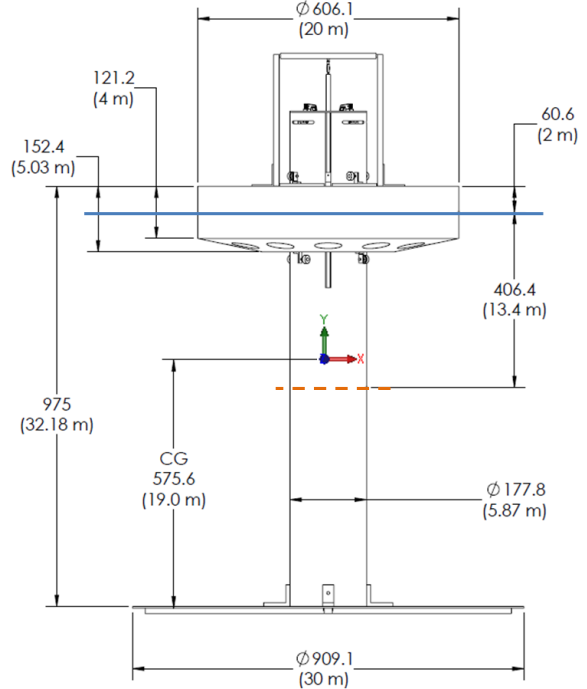| Component		Model Scale Mass (kg)	Full Scale Mass (Tonnes)
A	Float	20.23	727.0
B	Reaction Plate & Column	12.38	444.9
C	Column Ballast	9.70	348.6
D	Power Take Off (PTO)	3.24	116.4
E	Linear Pot 2	0.08	2.8
total		45.63 kg	1639.7 Tonnes

Figure 3 – Model Dimensions & Two Body CG, Model Scale Dimensions in mm, Full Scale dimensions in parentheses.
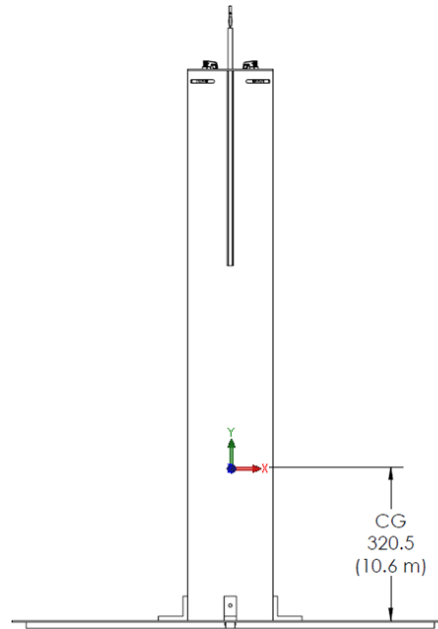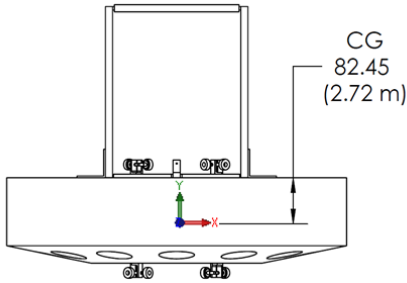

Figure 4 – Column & Reaction Plate CG

2

Figure 5 – Surface Float CG

Table 2 - Model Inertia Breakdown, Z component is normal to figures.

	Inertia Model Scale (kg m2)	Inertia Full Scale (kg m2)
	Surface Float	
Ixx	0.534	2.090E7
Iyy	0.948	3.710E7
Izz	0.544	2.129E7
	Column & Reaction Plate	
Ixx	3.515	1.376E8
Iyy	0.728	2.849E7
Izz	3.514	1.375E8
	2 Body Model (locked PTO)	
Ixx	7.727	3.024E8
Iyy	1.676	6.559E7
Izz	7.737	3.028E8

The mooring system was represented by matching the global spring stiffness in surge of the mooring system using a set of 4 springs that were separated by 90 degrees around the model. At full scale, the 3-leg mooring system has a spring stiffness of 103 kN/m or 94.6 N/m at 1:33 scale. To match the global spring-stiffness using a four-leg mooring system, the actual spring stiffness used was 61.3 N/m.
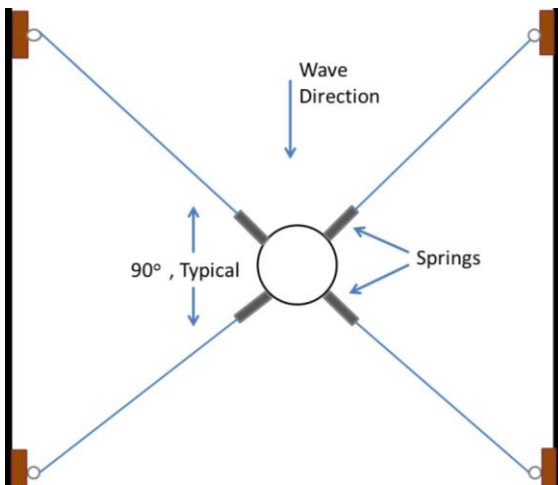

Figure 6 – Mooring Setup (Top View)

The measured effective spring-stiffness of the model in the wave tank is 260 kN/m. This value is slightly higher than the full-scale mooring design, which has an effective stiffness of 208 kN/m.

Previous tests showed that having a predictable damping term representing the power take off is important to systematically test the system. A custom damper was designed, consisting of a plate that is immersed in water. Different size orifices within the plate were opened or closed to attain desired damping values.
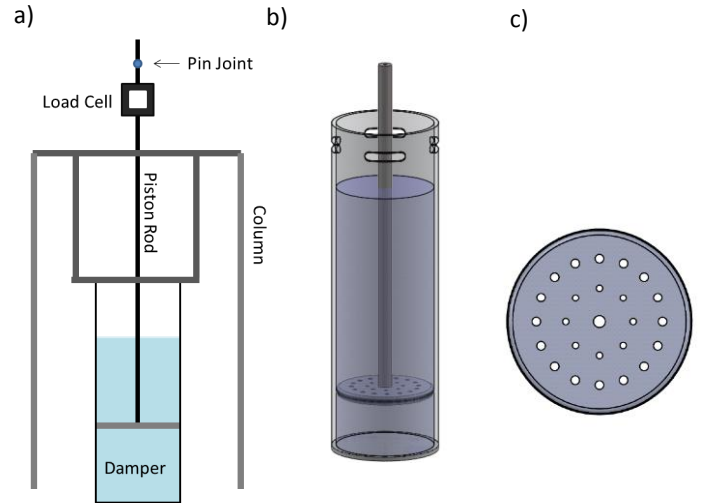

Figure 7 – Custom power-take off and load cell. a) schematic configuration of device, b) piston setup, and c) orifice configuration on the piston

Motions of the model were recorded using an OptiTrack camera tracking system provided by the National Renewable Energy Laboratory (NREL). Six cameras were used for the testing and were arranged around the model with two on each side wall of the tank and two closer to the wave maker. The overlapping field of view from each camera combine to make the motion capture volume.
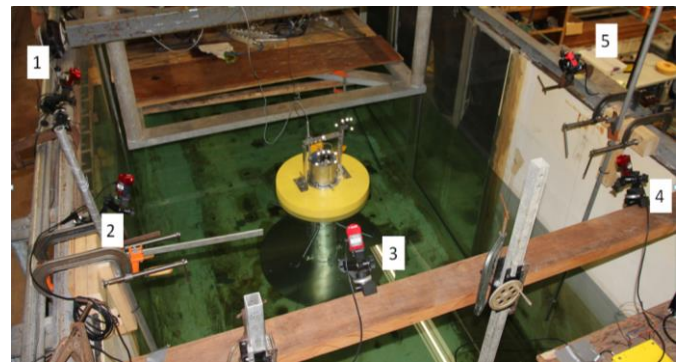

Figure 8 – Typical Camera Layout for Testing, Camera 6 not shown

The tracking system allowed for the independent tracking of the absorber float and the reaction plate. Two separate tracking objects (Trackables) were mounted to the float and the column and their motion was recorded by the system at 100 frames per second. The relative motion between the absorber float and reaction plate was also measured using a linear potentiometer that provided a validation of the optical tracking system.

For the test, the model was equipped with a linear potentiometer and load cell to measure the relative motion and force between the column and float and to compute mechanical power absorbed. Mooring line loads were measured using a load cell on one of the mooring lines. An inductance wave probe located 2m up-wave of the model measured the incoming wave profiles. The signals were recorded and scaled using LabVIEW and the time records have been transferred into a Matlab data file to simplify the analysis of the signals. A 4Hz low-pass digital filter was used to remove any noise from the signals obtained from the measurements.

Computational Model Parameters

To compare the experimental and numerical results, the key characteristics of the experiments are used as input parameters for the numerical model. According to DNV Recommended Practice [2], to validate the current model the following items are calibrated and checked:

- model characteristics (geometry, mass, mass distribution, metacentric heights, waterline),
- restoring force stiffness/damping forces,
- natural periods in heave/surge/pitch degrees of freedom (in water),
- check of instrumentation; sensor characteristics; accuracy levels.

Modeling of the system was done using the commercial code AQWA, and an in-house code Re-WEC that Re Vision uses for commercial projects. Both of the codes utilize boundary element methods to compute hydrodynamic responses in the time-domain and allow for the introduction of external forces coming from viscous drag, mooring lines and power take off system.

In order to allow for an accurate comparison between the theoretical model and the measured results, the theoretical model had to reflect the exact conditions of the model tests carried out. The Center of Gravity (CG), Mass and Moment of Inertia, were chosen based on the model properties at full scale using Froude scaling laws.

The measured wave height time series from the wave measurement probe located 2m in front of the buoy was used to create the input wave time histories the models. A sinusoidal wave that best fit the measured wave height was used as the input time series for numerical analysis. The computed wave profiles were similar to the measured profiles, but did not include the sharper wave crests and wider wave troughs caused by higher order effects and observed at the wave tank. From a sensitivity analysis, it was found that the higher order effects were not important factors for the wave periods of interest.

Small errors in wave amplitude or period caused by the wakemaker were accounted for by processing the wave time histories and computing the spectrum of the measured waves. In Figure 9, the spectra of the recorded wave history from one test and the corresponding sinusoidal best fit used in the numerical analysis are shown.
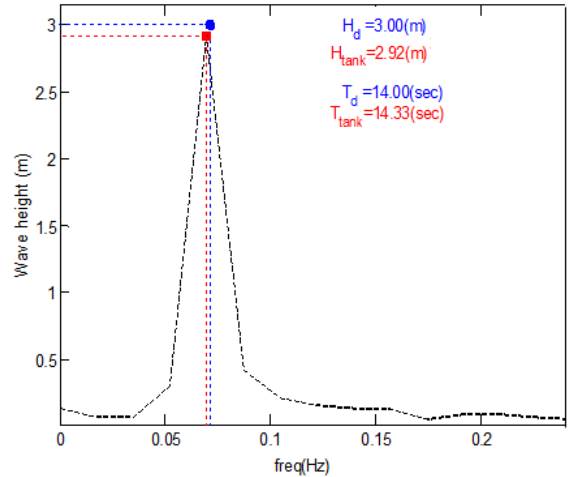

Figure 9 – Recorded wave spectra and obtained harmonic wave (sample case with T=14 sec), additional frequencies not shown.

Morrison-type drag terms were added to account for losses due to viscous effects. Use of the appropriate drag-terms proved to be important to appropriately match the theoretical results to the model behavior. There is an implicit assumption that the differences in observed and modeled quantities can be represented by these terms and issues such as wall-effects in the wave tank have negligible effects on the device performance. The following table summarizes the drag-terms used.

Table 3 – Drag Coefficients (CD) Used for Models

	Heave	Surge	Pitch
Absorber Float	0.0	0.0	0.0
Central Column	0.0 in local coordinate	0.65 ψ(KC) in local coordinate	Related to translational drag coefficients (refer to the following discussion)
Reaction Plate	KC dependent (>3.0 , <5.0) Initial guess = 4.5	Linear damper (equivalent to the drag coefficient ~ 0.03)	

The drag coefficient in oscillatory flow was related to the drag coefficient in steady unidirectional flow using as a function of the KC number from DNV recommended practice RP-C205 [2]. The KC number is defined as

$$KC = \frac{U_A T}{L},$$

where U_A is the amplitude of relative velocity of fluid with respect to structure, T is the main period of oscillation (the period of the incoming wave) and L is the characteristic length scale. Figure 10 shows the relationship between drag amplification factor of a circular cylinder and KC number.
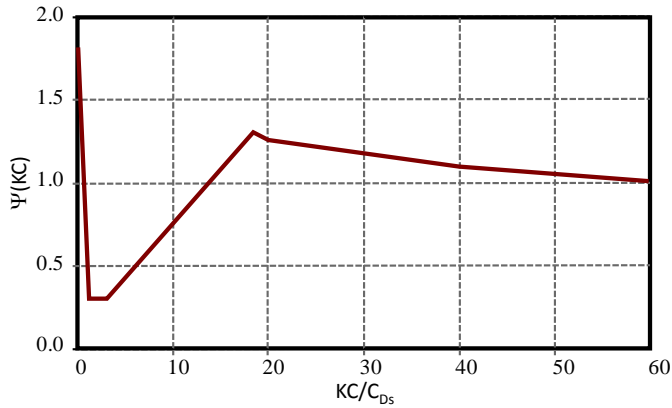
4

Figure 10 – Wake amplification factor as a function of KC number for a smooth cylinder $C_{Ds}=0.65$

The viscous drag forces on the column are included through viscous part of the Morison's equation. The inertial part is eliminated because it is included in the total hydrodynamic forces calculated from our boundary integral approach. To find the viscous forces on the column, kinematic stretching was used to predict the fluid velocity at the column center at different heights on the column.
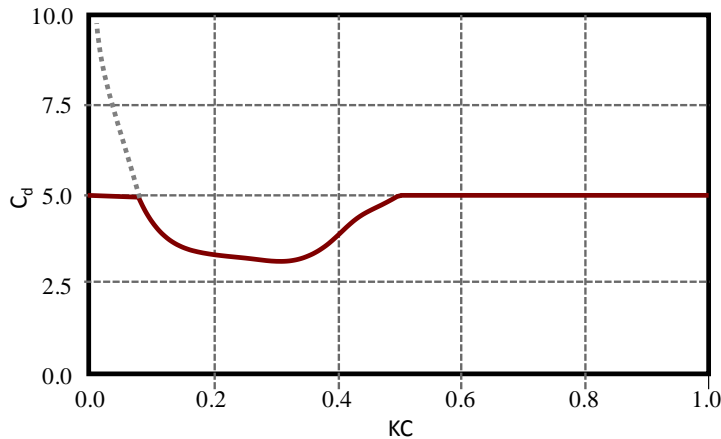

Figure 11 – Drag Coefficient of the reaction plate in heave direction as a function of KC number.

To obtain an estimation of the drag coefficient of the reaction plate, experimental results from He, Troesch, and Perlin [4] for moderately thin plates were used. The maximum allowable drag coefficient was chosen to be 5.0 since higher values of the drag coefficient only occur at very small KC numbers in which the reaction plate has a very small velocity and hence does not impact reaction plate motion. Figure 11 shows the relationship between drag coefficient of the plate and KC number. To insure proper representation of the drag forces on the reaction plate, we placed the point-forces (resulting from the drag) on the reaction plate's edge, assuming the drag force was a result of vortices produced by the plate edge as observed through visualization techniques (injection of color) in the wave tank.

More specifically, drag coefficient per unit area of the plate normal to heaving direction were converted to one per unit length of the plate perimeter and second by computing point-wise drag coefficient based on the velocity of each point along the edge of the reaction plate. Since the drag coefficients of the column and reaction plate were related to initially unknown column and plate oscillation amplitude, an iterative

approach was used to determine drag as a function of KC number. The results typically converged within two or three iterations and the final C_D values were similar to the initial mean values and needed only minor corrections. The cumulative impact of the correction had only a secondary effect on the final results.

The surge motion of the reaction plate, also created drag forces similar to a low Reynolds number airfoil (at small angle of attack) because of the oblique orientation of the plate. This behavior was modeled by a very small linear damper attached to reaction plate (equivalent to the drag coefficient ~ 0.03).

For the mooring setup in the numerical model, we used the designed effective stiffness from the full scale model, which closely represents the model spring-stiffness.

AQWA Model Results

To simulate the experimental condition, two numerical models were developed. In the first model, the device is constrained to only move in the heave direction, hereafter is also referred as 1DoF model. In the second model, the model was allowed to move in surge, heave and pitch. In the remaining sections this model is referred as 3DoF model. Damping effects were included in the AQWA model through an external dll library, which allows external time-dependent forces to be applied to the system. The same dll file was used to record the performance output and the responses of the system during the simulation. For the 3DoF cases the reaction plate and column were treated as a single structure and the heaving buoy as a second structure constrained to move against each other in only one direction.

The following figures show the modeled and measured power outputs as a function of damping value applied to the power take off. The comparison has been made between the experimental, 1 DoF, and 3 DoF numerical model mean power output vs. the damping values.
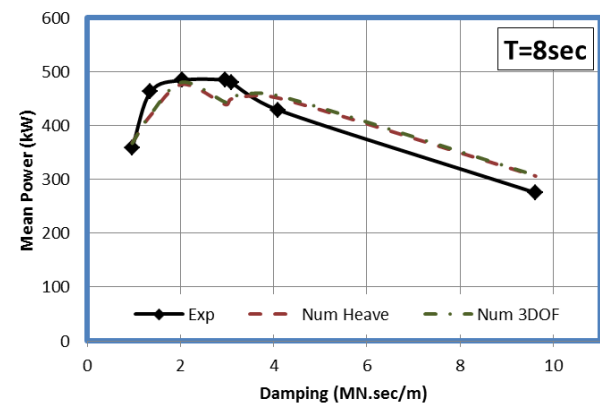

Figure 12 – Numerical Model and Experimental Damping vs. Mean Power at T = 8 sec.
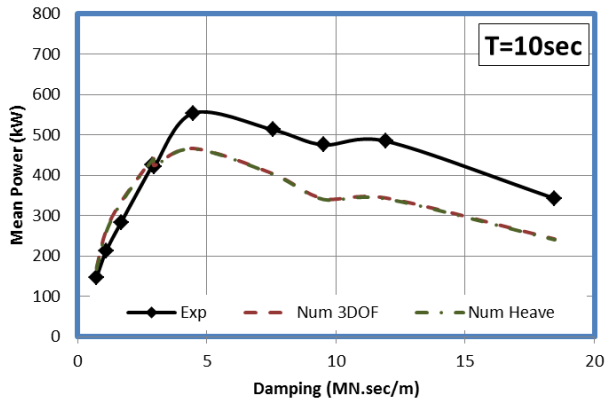
5

Figure 13 – Numerical Model and Experimental Damping vs. Mean Power at T = 10 sec.
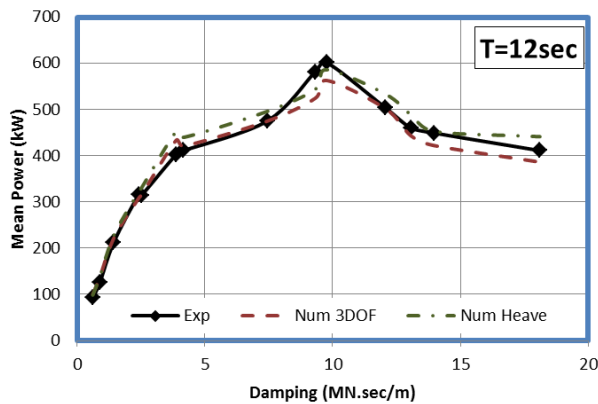

Figure 14 – Numerical Model and Experimental Damping vs. Mean Power at T = 12 sec.
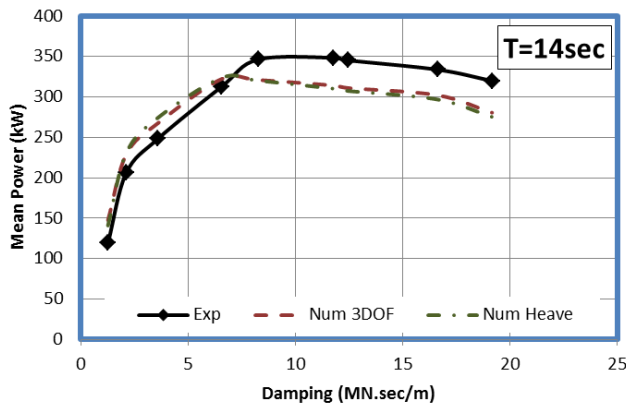

Figure 15 – Numerical Model and Experimental Damping vs. Mean Power at T = 14 sec.

The numerical results match well with experimental observations especially for the case with larger contribution on the mean power (T = 8 to 12 sec). As wave period is increase towards 12 seconds, the maximum mean power increases and shifts to higher damping values as expected. Above 12 seconds and in the longer wave periods, a lower peak average power is measured and modeled because the two bodies move together reducing their relative displacement.

Figure 17 shows measured and computed power output using the optimal damping terms applied to the power take off. As presented in Figure 1716, the optimal damping increases from c~1.2 MN.sec/m at T=6sec to c~10 MN.sec/m at T=12sec and decreases to c~6 MN.sec/m at T=18sec. The results show good correlation between experimental observations and numerical predictions. It should be mentioned that the performance is for regular wave conditions and the optimal power output will be changed for more realistic irregular wave conditions with broader spectrums.
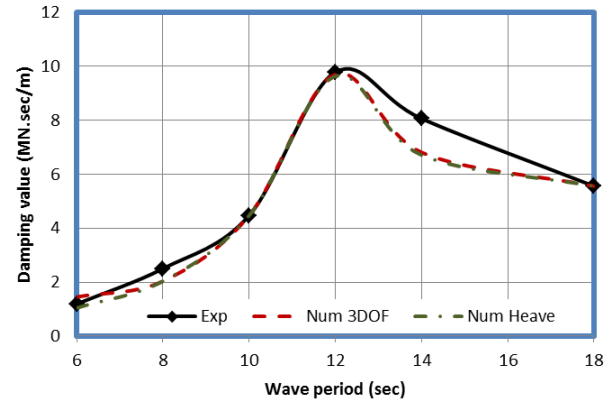

Figure 16 – Changes of optimal damping value as a function of wave period.
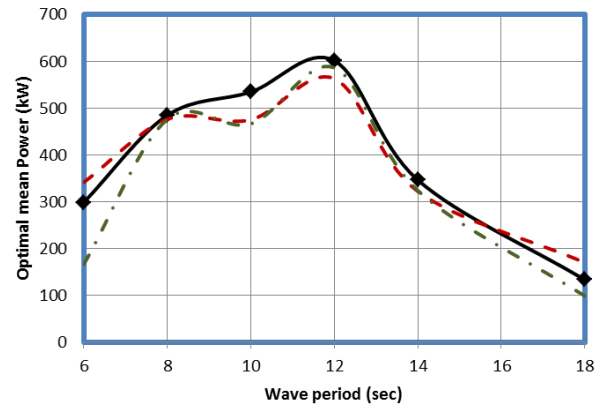

Figure 17 – Changes of maximum mean power output as a function of wave period.

The reaction plate design is critical for this type of device to maximize device performance. The amount of viscous drag of the plate moving in vertical direction can be influenced by rounding the edges of the reaction plate, hence reducing it's coefficient of drag and related viscous losses. To study this effect, the drag coefficient of the reaction plate was varied in the computational model to study the performance increase at different wave periods.

Across the wave periods where the model predicts the highest power output (10-14 sec), the maximum mean power output decreases as the reaction plate drag coefficient increase. The performance drop off is most pronounced at T=12sec because the device is near resonance.
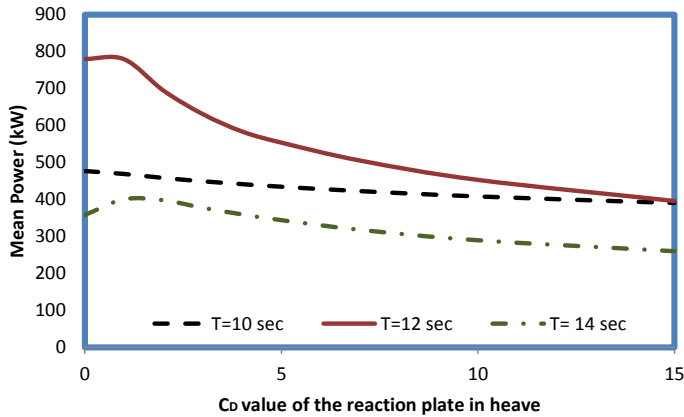
Figure 18 – Changes of the maximum mean power output as a function drag coefficient of the reaction plate in heave direction for different wave periods (T=10, 12 and 14 sec).

Wave to Wire Model

The performance given by the numerical approach described above only computes the average mechanical power the system produces in each sea-state. In order to establish how much electrical power can be fed into the grid, a simple wave to wire model was used to account for performance reductions.

Once the average device power was evaluated for each sea-state by use of the numerical model, this value was then multiplied by the frequency of re-occurrence given by the scatter diagram for the site. The following table shows the frequency distribution of sea-state reoccurrence at the sample reference site.

Table 4 - Scatter Diagram for Northern California Site

		Te (sec)							
		5	7	9	11	13	15	17	19
Hs(m)	**0.75**	3	13	14	4	4	6	5	1
	1.25	11	37	60	15	14	13	8	1
	1.75	6	46	65	25	22	15	7	2
	2.25	2	32	56	29	30	19	8	3
	2.75	0	14	46	23	30	21	9	3
	3.25	0	5	33	13	24	20	8	3
	3.75	0	2	17	7	16	18	7	2
	4.25	0	0	8	4	9	14	6	1
	4.75	0	0	3	2	5	10	5	1
	5.25	0	0	1	1	2	6	4	1
	6.25	0	0	0	0	1	5	5	1
	8	0	0	0	0	0	1	2	0

Device rated capacity, availability, and power conversion losses were superimposed onto the device performance results. Device rated capacity was iteratively determined so that the capacity factor of the

device yielded exactly 30%. Furthermore, the following assumptions were made to determine the annual energy production:

Power Conversion System Efficiency	80%
Plant Availability	95%
Transmission Efficiency	98%

The net average electrical power produced by the device is 87.2 kW, with a rated capacity of the device of 290 kW and a capacity factor of 30%. The following figure shows the trade-off between a devices rated capacity and the annual output in MWh/year.
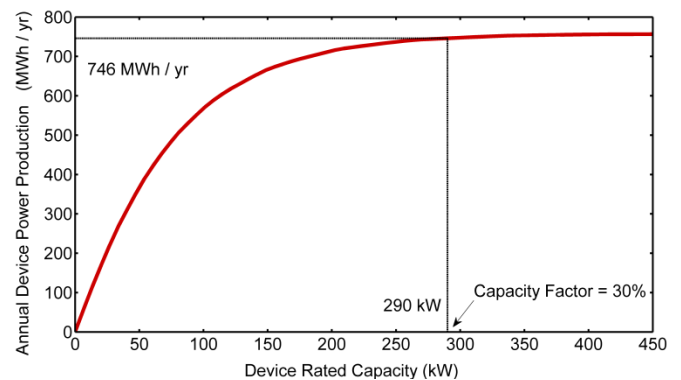

Figure 19 – Computed annual power production (MWh/year) from the device as a function of the device rated capacity (KW). The capacity factor happens at the rated capacity equals to 290 kW.

Sensitivity Studies

In order to understand the device performance sensitivities to design parameters, sensitivity studies were used to quantify the device performance impact of a particular design change. Initial results suggest that the performance of the studied device is very sensitive to; (1) water depth, (2) reaction plate viscous drag, and (3) control strategy. An example follows.

The viscous damping of the reaction plate can be influenced by design. I.e. the edges of the plate can be rounded to reduce drag. Figure 20 shows the device performance for different drag coefficients applied to the reaction plate. It shows that performance can be significantly improved if the reaction plate features rounded edges.
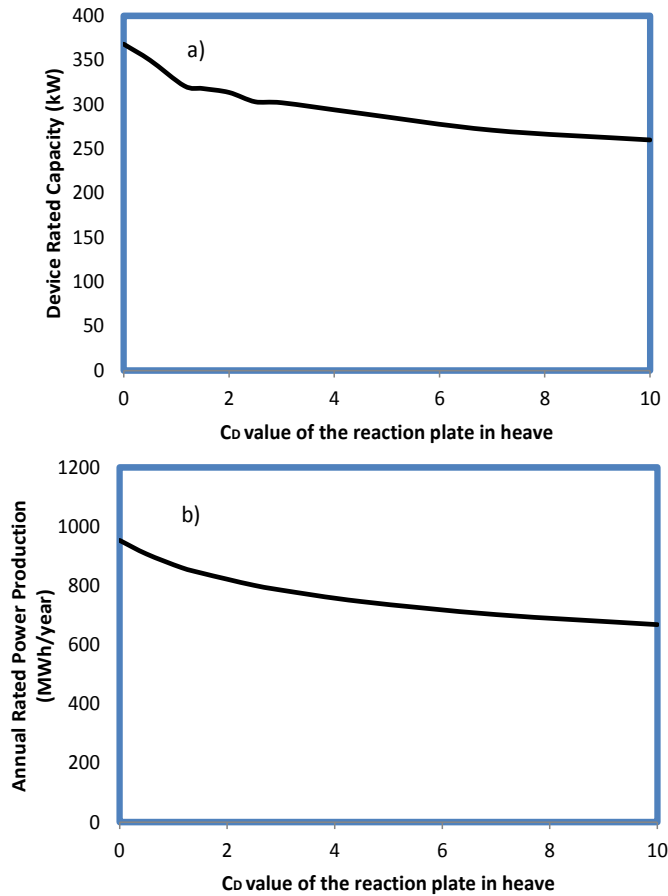
Figure 20 – Computed a- the device rated capacity and b-annual power production (MWh/year) as a function of drag coefficient of the reaction plate.

Conclusions and Next Steps

The code-validation carried out under this program shows good correlation between measured data theoretical models that are based on the Boundary Element Method (BEM).

A 1:33 scale model of the device was tested from November 30th to December 2nd 2011 at the Scripps Institution of Oceanography wave tank. The goal for the experiment was to validate the computational models and provide confidence in the device performance estimates used. A novel linear viscous damper was used to model the power-take off. Due to the limitations of the wave tank, tests were carried out using only sinusoidal waves. Given that the primary purpose of these tests was to validate the theoretical performance models during this conceptual-level development, this was considered to be sufficient.

Now that a validated theoretical model is in place, further design trade-offs should be studied to fully optimize the overall system design. The following measures show promise in respect to quantifying the device performance:

1. Performance validations were carried out using only sinusoidal waves. This was largely due to the limitations of the wave tank, which allows for limited controls. A next set of validation tests should be carried out in irregular seas to complement the existing performance data set.
2. Advanced rapid tuning strategies have shown to hold significant potential for this type of device. Using the existing codes, these tuning strategies could be evaluated. Additional wave tank testing would likely be required to validate these strategies.
3. This study has shown that reducing the drag coefficient of the reaction plate can improve power capture significantly. This could be accomplished by rounding the edges of the reaction plate, hence reducing flow-separation around the plate edges.
4. In this study, we used a standard PM spectrum. Evaluating the sensitivity of the device performance to the spectral distribution by using a site-specific spectrum will be important in quantifying the uncertainty surrounding these performance predictions.

References

1 Cummins, W.E. (1962), The Impulse Response Function and Ship Motions, *Department of the Navy Hydromechanics Laboratory Research and Development Report.*

2 DNV Recommended Practice, DNV-RP-C205, Environmental Conditions and Environmental Loads, 2007.

3 Falcao AF de O (2009), Wave energy utilization: a review of technologies, *Renewable and Sustainable Energy Reviews,* 14(3): 899-918.

4 He, H., A. Troesch, and M Perlin (2007), Hydrodynamics of damping plates at small KC numbers, *IUTAM Symposium on. Fluid-Structure Interaction in Ocean Engineering.*